Results in Physics 9 (2018) 1185–1191

Contents lists available at ScienceDirect

Results in Physics

journal homepage: www.elsevier.com/locate/rinp

Numerical analysis of installation damage of a pre-damaged geogrid with rectangular apertures

Yan-li Dong[a,b,c,*], Hui-juan Guo[a], Jie Han[c], Jun Zhang[b]

[a] Civil Engineering, School of Science, North University of China, Taiyuan 030051, Shanxi, China
[b] Key Laboratory of Highway Construction and Maintenance Technology in Loess Region, Ministry of Transport, Shanxi Transportation Research Institute, Taiyuan, Shanxi 030006, China
[c] Department of Civil, Environmental, and Architectural Engineering, The University of Kansas, Lawrence, KS 66045, USA

ARTICLE INFO

Keywords:
Geogrid with rectangular apertures
Installation damage
Tensile strength retained
Reduction factor
Tensile strength distribution

ABSTRACT

The geogrid can be damaged in the process or during construction if sufficient care is not exercised. In this study, the numerical software-FLAC was adopted to investigate the responses of pre-damaged geogrids with rectangular apertures when subjected to a uniaxial tensile load at different directions relative to the orientations of ribs in air. To simulate the combined loss of ribs and junction strength, specimens were pre-damaged by reducing certain amount of stiffness of the geogrid ribs. The geogrid ribs were modeled using beam elements jointed rigidly at nodes and subjected to tension in one direction. The numerical study demonstrated that the pre-damaged geogrid with rectangular apertures had similar responses when it was subjected to tension at the loading directions. The pre-damaged geogrids under 30° tension are the most sensitivity to the damage. With the increase of the degree of damage, the tensile strengths decreased relative quickly. An increase of the degree of installation damage of ribs decreased the tensile strength/stiffness of the geogrid with rectangular apertures. A higher reduction factor RF_{ID} due to installation damage is suggested when the geogrid is subjected to 30° tension relative to the orientation of ribs.

Introduction

Geogrids have been successfully and widely used in many engineering projects. The use of geogrids may be associated with the use of heavy machinery for construction of reinforced structures. The geogrid can be damaged in the process if sufficient care is not exercised. The placement and compaction of fill material during construction may also result in damage. Some damage is likely unavoidable and must be taken into account in design as a matter of routine. The investigation of installation damage of geogrids using full-scale field tests has been performed since 1980s (for example, [1,13,12,14,5]). It has shown that, the extent, severity and type of damage depend on the degree of care exercised during the construction, the type and number of passes of machinery employed [14], the graduation, angularity and condition of the fill material [13,12,5]. Laboratory tests on installation damage of geogrids are preferred considering time and cost-effectiveness, such as those performed by Paula et al. [11], Hufenus et al. [10], Huang and Chiou [7], Huang [6], and Huang and Wang [8]. Therefore, it is practically impossible to predict the actual manner and extent of damage that a given reinforcement may suffer under all construction conditions.

Furthermore, biaxial geogrids were used to carry tensile force in one or two directions along the ribs due to apertures shape (i.e., rectangular or square). Almost all the tensile and pullout tests of the geogrid especially for the damaged specimen have been conducted in the directions same as the orientations of the geogrid ribs (i.e., machine and cross-machine directions). In real applications, however, applied loads may not necessarily follow the orientations of these ribs, for example, traffics on construction sites and parking lots. How the damaged geogrid responds if subjected to a tensile load at a direction different from the orientations of biaxial geogrid ribs is not well understood.

Considering the variability involved, a numerical method was adopted in the present study to evaluate the effect of installation damage upon the tensile strength of a given geogrid with rectangular apertures when subjected to a uniaxial tensile load at different directions relative to the orientations of ribs in air. The proposed method does not address the susceptibility of a geogrid to damage, but rather it focuses on the effect of a certain amount of damage on the tensile strength. It will be seen that even a relatively large amount of damage to the geogrid ribs does not substantially affect the tensile strength of the geogrids used in this investigation. The reason for selecting a uniaxial loading test is that this test is the most common method to evaluate the stress-strain behavior of geosynthetics.

* Corresponding author at: Civil Engineering, School of Science, North University of China, Taiyuan 030051, Shanxi, China.
E-mail addresses: qianxinjie@yahoo.com, dyli82@sina.com (Y.-l. Dong), jiehan@ku.edu (J. Han).

https://doi.org/10.1016/j.rinp.2018.04.016
Received 24 September 2017; Received in revised form 6 January 2018; Accepted 8 April 2018
Available online 13 April 2018

As stated earlier, the amount and type of damage caused on a geogrid in actual construction are random in nature. To simulate the combined loss of ribs and junction strength, specimens were pre-damaged by reducing the strength and stiffness of the geogrid ribs by a certain amount. For the comparison purpose, the geogrid specimen of the same dimension without any damage was also simulated.

This paper focuses on the quantitative evaluation for the reduction factor due to installation damage of a geogrid with rectangular apertures using the numerical method.

Numerical modeling

In this study, the software FLAC 2D was used to evaluate the behavior of a pre-damaged geogrid with rectangular apertures. For the application of the finite difference software - FLAC (Fast Lagrangian Analysis of Continua) 2D, Han and Gabr [4] considered the geosynthetic reinforcement as linear elastic material. Huang et al. [9] used cable elements to model the geosynthetic reinforcement. Dong et al. [2] used beam elements to investigate the stress-strain responses of biaxial geogrids under tension. Dong et al. [3] used the same beam elements to simulate the tensile behavior of both biaxial and triaxial geogrids.

Model considerations

With a linearly elastic-perfectly plastic behavior, beam elements with a large-strain mode were selected to represent the rib of the pre-damaged geogrid sample. All the nodes of beam elements were jointed rigidly to form apertures and a geogrid sheet.

To model a geogrid sample at different installation damage conditions, certain degree of damage was assigned to the geogrid ribs. Only the geogrid ribs in the middle of the whole test sheet along the cross-machine direction (XMD direction) was pre-damaged (i.e., the red line in the middle as shown in Fig. 1). The numerical analyses of the tensile behavior of these cases under tension will be presented in the following section. The degree of damage was mainly determined by reducing the ultimate tensile strength of the assigned geogrid ribs to a desired value (i.e., 0%, 25%, 50%, and 75% reduction of the ultimate tensile strength). The geogrid sheet was rotated around a fixed centroid to a desired angle (0, 45, 60, and 90°) to model a pre-damaged geogrid specimen subjected to an uniaxial tensile load at a different direction. The geogrid specimen without any damage (i.e., the degree of damage equals to 0) was also simulated for the comparison purpose.

A mesh size of 330 mm by 200 mm for the whole specimen (the minimum size of geogrid sample required by ASTM D6637-01 for a geogrid tensile test was 300 mm by 200 mm) was selected to accommodate complete apertures for the pre-damaged geogrid specimen for this analysis. The aperture size was selected based on a real geogrid with rectangular apertures, available in the market. The detailed physical properties are listed in Table 1.

Table 1
Physical properties of the geogrid presented in this paper.

Parameters	Aperture Dimensions (mm)	Minimum Rib Thickness (mm)	Tensile Strength @ 2% Strain (kN/m)	Ultimate Tensile Strength (kN/m)
MD Values	25	1.27	6.0	19.2
XMD Values	33	3	9.0	28.8

As stated in ASTM D6637-01, the specimen was gripped across its entire width in the clamps of a constant rate of extension type tensile testing machine operated at a prescribed rate of extension, applying a uniaxial load to the specimen until the specimen ruptures. Tensile strength (kN/m), elongation, and secant modulus of the test specimen can be calculated from the test data.

To simulate a laboratory tensile test of a geogrid sample, the geogrid mesh for numerical analysis was created by fixing the movement in x and y directions at the left boundary as shown in Fig. 1. The movement in the y direction was fixed but not in the x direction at the right boundary. The rotation around each node was not allowed. Fig. 1 shows the numerical mesh for the pre-damaged geogrid oriented in a 0-degree angle (i.e., the cross-machine direction of the geogrid) as an example. On each node on the right boundary, an equal velocity at 5e-8 m/step was applied horizontally until the failure. This loading direction was considered as 0-degree tension direction.

Model verification

The model parameters were determined based on the physical properties listed in Table 1. Fig. 2 shows the comparison of numerical and test results of the geogrid under 0 and 90°tension. This comparison verified the reasonability of the numerical model. Detailed information about this verification can be found in Dong et al. [2].

To investigate the effect of the tensile stiffness and strength, a simplified geogrid with the same material parameters in MD and XMD was used in this study. Detailed discussion on this simplification can be found in Dong et al. [3]. The simplified geogrid model with rectangular apertures was also used in this study. The parameters used in this study

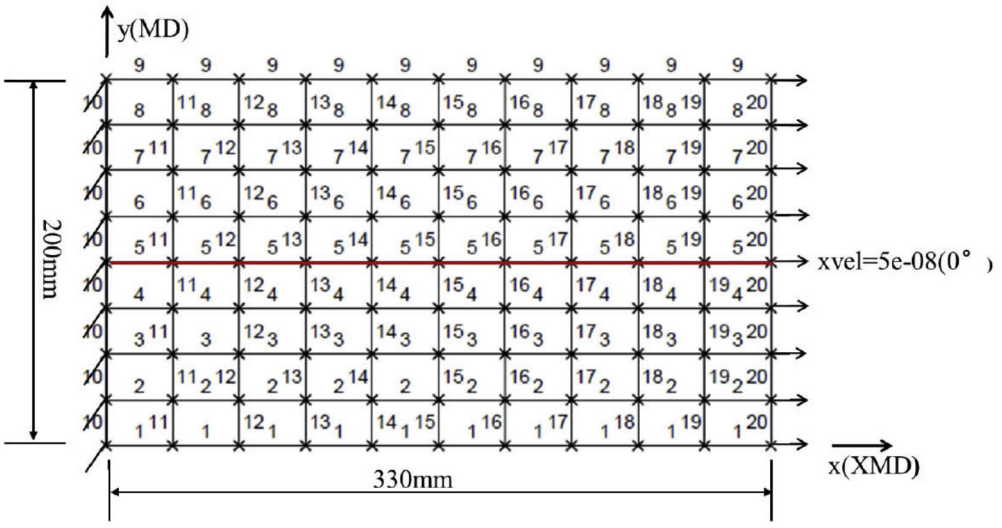

Fig. 1. Meshes of a pre-damaged geogrid with rectangular apertures (with numbers).

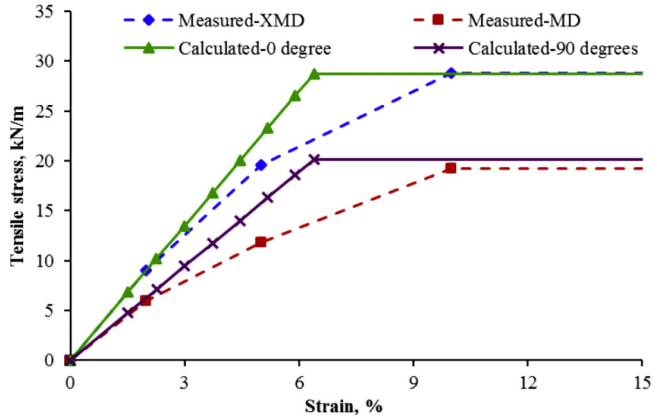

Fig. 2. Comparison of numerical and test results of the geogrid with rectangular apertures at 0 and 90° [2].

Table 2
Parameters of the numerical models presented in this paper.

Type	Degree of damage (%)	Cross-section area of ribs (10^{-6} m^2)	Moment of inertia (10^{-12} m^4)	Elastic modulus (MPa)	Yield strength (MPa)
B-0	0	3.81	0.512	2625	168
B-25	25	3.81	0.512	1969	126
B-50	50	3.81	0.512	1313	84
B-75	75	3.81	0.512	656	42

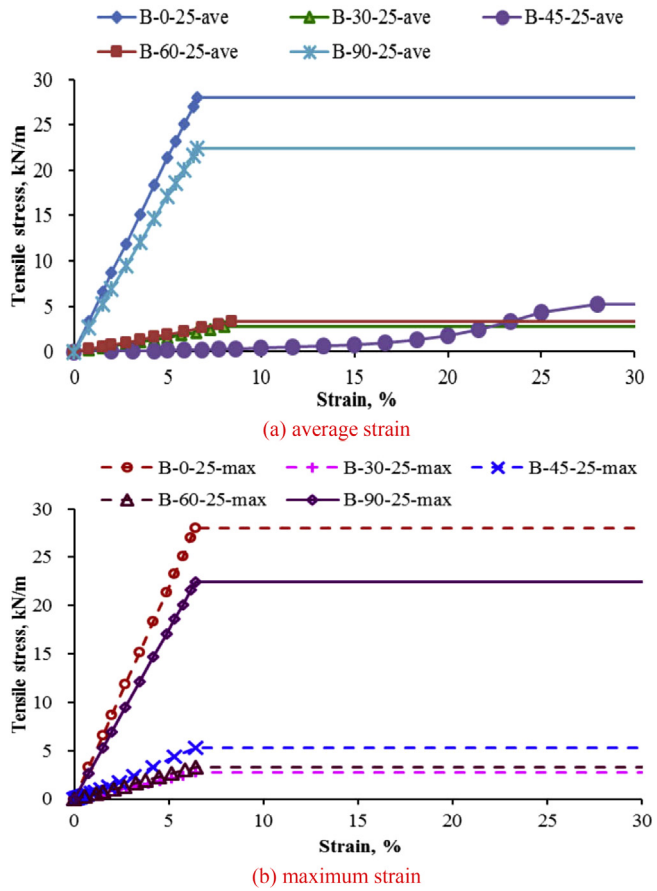

Fig. 3. Stress- strain curves of pre-damaged geogrid of 25% degree of damage with rectangular apertures at all loading directions.

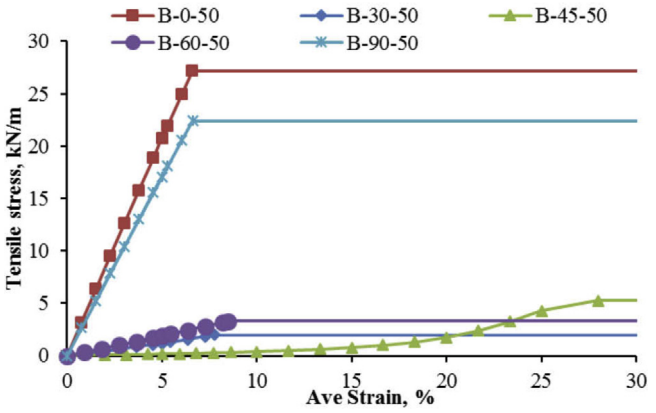

Fig. 4. Stress- strain curves of pre-damaged geogrid of 50% degree of damage with rectangular apertures at all loading directions.

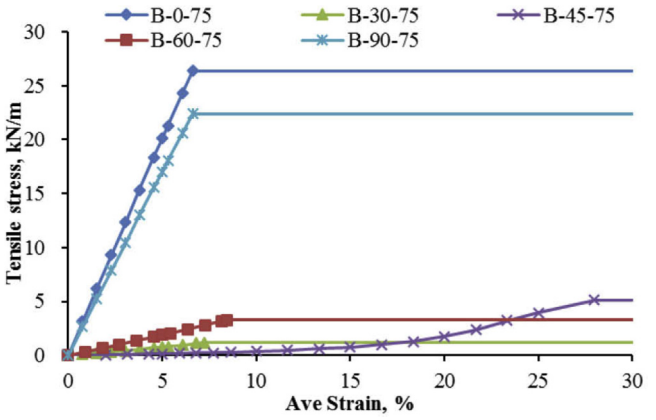

Fig. 5. Stress- strain curves of pre-damaged geogrid of 75% degree of damage with rectangular apertures at all loading directions.

are provided in Table 2. The geogrid is designated as Geogrid B together with a pre-damaged degree (i.e. B-0, B-25, B-50, and B-75). Here, the pre-damaged degree means the degree of the damaged geogrid specimen due to installation damage. As a practical point of view, it means the loss of tensile strength of geogrid due to installation damage. All the geogrids had the same cross-section area of ribs and moment of inertia with the value of 3.81×10^{-6} m^2 and 10^{-12} m^4, respectively. Geogrids B-25 had a 25% reduction of both elastic modulus and yield strength as compared with Geogrid B-0.

Numerical results and analysis

The degree of damage was mainly determined by reducing the ultimate tensile strength of the assigned geogrid ribs to a desired value (i.e., 0%, 25%, 50%, and 75% reduction of the ultimate tensile strength). The loss of tensile strength due to damage was evaluated by the percentage of tensile strength retained (PT_R) and reduction factor (RF_{ID}) against installation damage. Here, the percentage of retained tensile strength (PT_R) is referred to the tensile strength of the pre-damaged geogrid specimen divided by the tensile strength of intact geogrid specimen times hundred percent. Reduction factor (RF_{ID}) is defined as the ratio of the tensile strength of intact geogrid specimen to the tensile strength of the pre-damaged geogrid specimen.

Stress-strain curves

The numerical results of the tensile behavior of the pre-damaged geogrids subjected to different tensile loading relative to the orientation of XMD ribs are summarized in the following figures. The first number

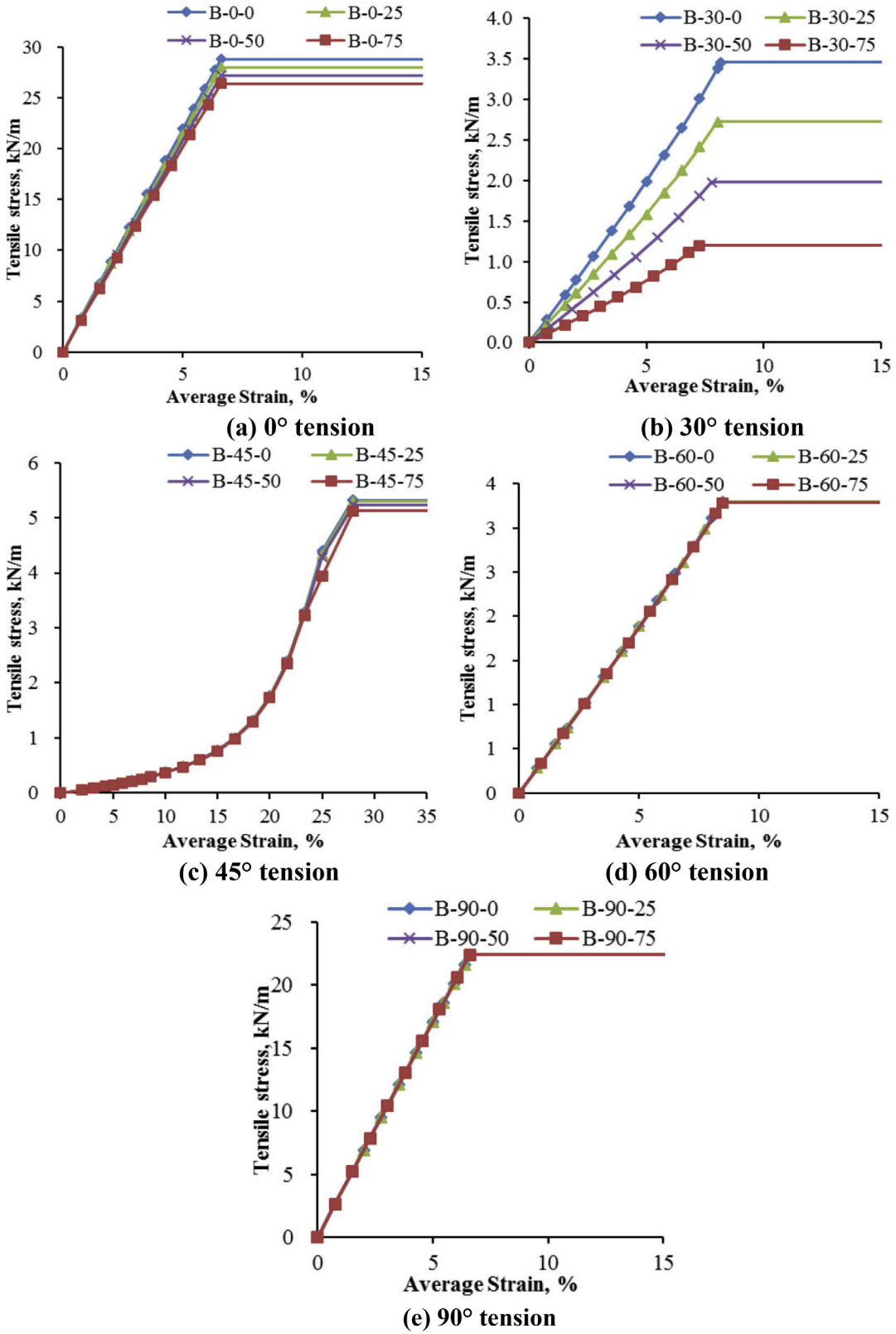

Fig. 6. Stress- strain curves of pre-damaged geogrid with rectangular apertures under different tension.

groups (i.e. 0˚, 30˚, 45˚, 60˚, and 90˚) in the figures represent the loading directions while the second number groups (i.e. 0, 25, 50, and 75) represent the degree of damage.

Effect of loading directions

Fig. 3 presents the stress-strain responses of the pre-damaged geogrids at 25% degree of damage. The solid lines in Fig. 3(a) are plotted using the average strain of the geogrid sample while the dashed lines in Fig. 3(b) are plotted using the maximum strain at yield. Here, the

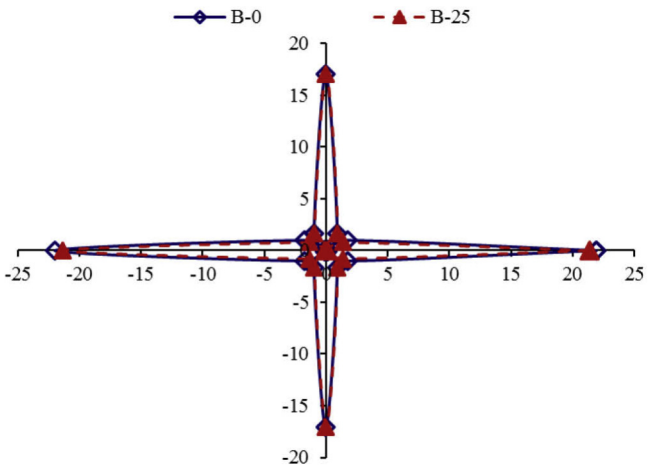

Fig. 7. Distribution of tensile strengths around 360° at 25% degree of damage (unit: kN/m).

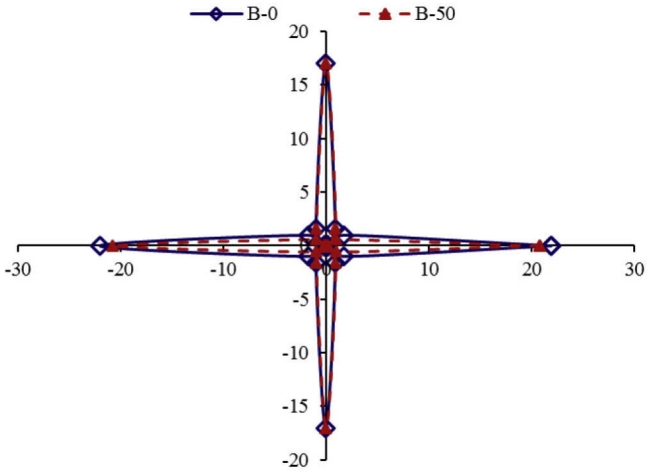

Fig. 8. Distribution of tensile strengths around 360° at 50% degree of damage (unit: kN/m).

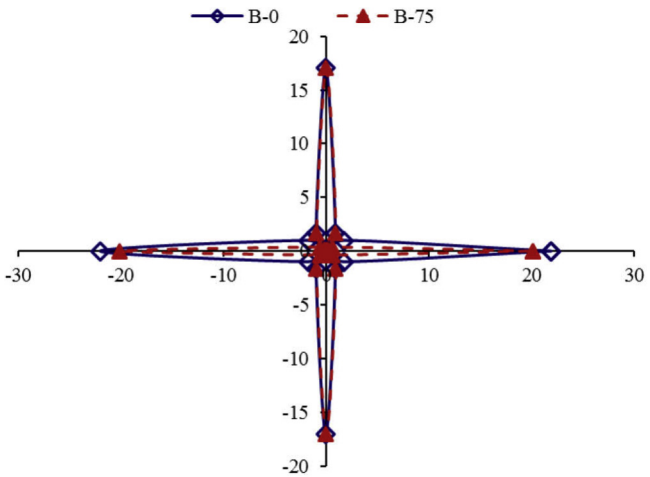

Fig. 9. Distribution of tensile strengths around 360° at 75% degree of damage (unit: kN/m).

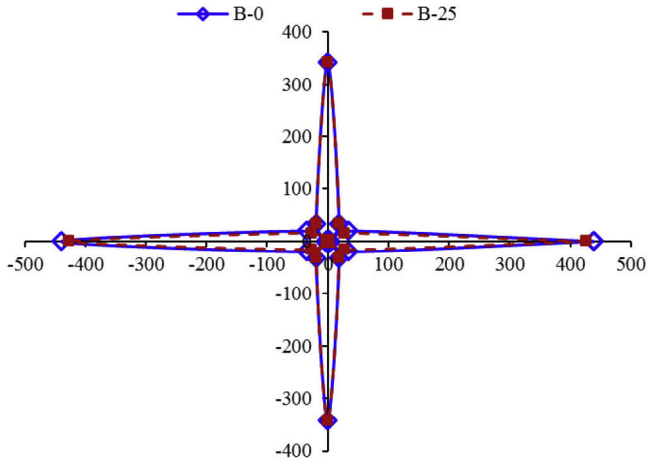

Fig. 10. Distribution of tensile stiffness around 360° at 25% degree of damage (unit: kN/m).

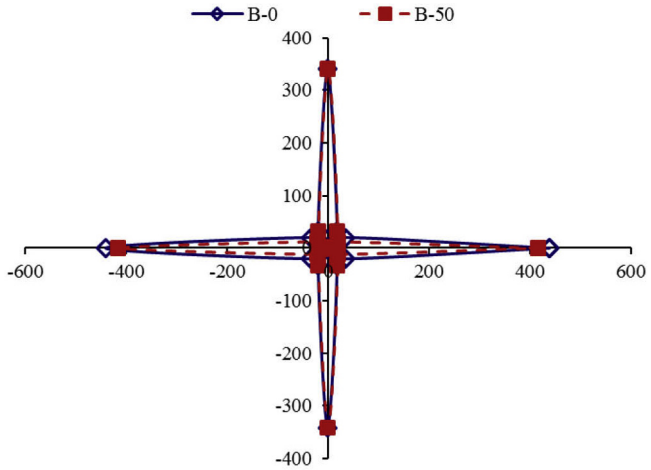

Fig. 11. Distribution of tensile stiffness around 360° at 50% degree of damage (unit: kN/m).

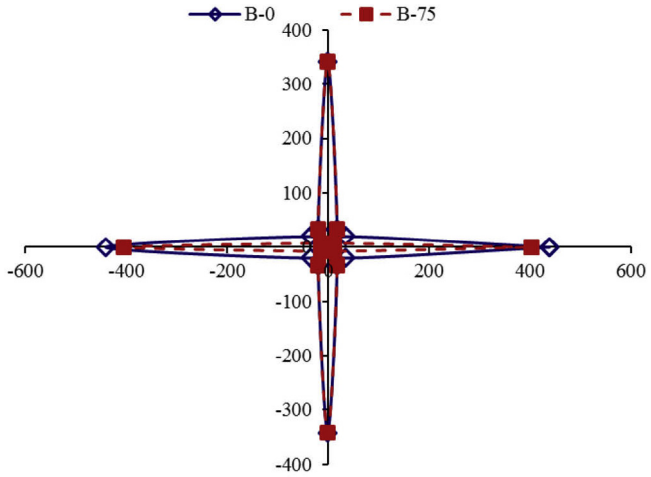

Fig. 12. Distribution of tensile stiffness around 360° at 75% degree of damage (unit: kN/m).

definition of the average strain was the value of the horizontal movement at the right boundary divided by the initial length of the sample. The maximum strain was defined as the largest strain mobilized among all the ribs in each geogrid sample. As shown in Fig. 3, the stress-strain curves for the pre-damaged geogrids at all loading directions are nearly the same, except for the 45-degree loading. Under 45-degree tension, the maximum strain of the pre-damaged geogrid sample was much smaller than the average strain due to necking. In the following sections of this paper, an average strain will be used for discussion.

Table 3
PT_R of the pre-damaged geogrid at all loading directions (%).

Tension Directions	Degree of Damage			
	0%	25%	50%	75%
0°	100	97	95	92
30°	100	80	59	37
45°	100	100	100	100
60°	100	100	100	100
90°	100	100	100	100

Table 4
RF_{ID} of the pre-damaged geogrid at all loading directions.

Tension Directions	Degree of Damage			
	0%	25%	50%	75%
0°	1.00	1.03	1.06	1.09
30°	1.00	1.25	1.70	2.69
45°	1.00	1.00	1.00	1.00
60°	1.00	1.00	1.00	1.00
90°	1.00	1.00	1.00	1.00

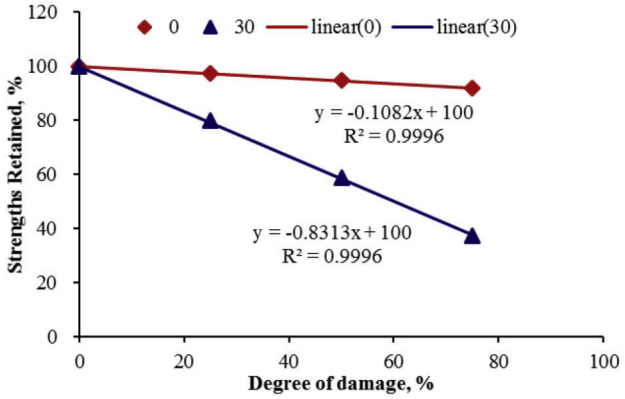

Fig. 13. PT_R against degree of damage.

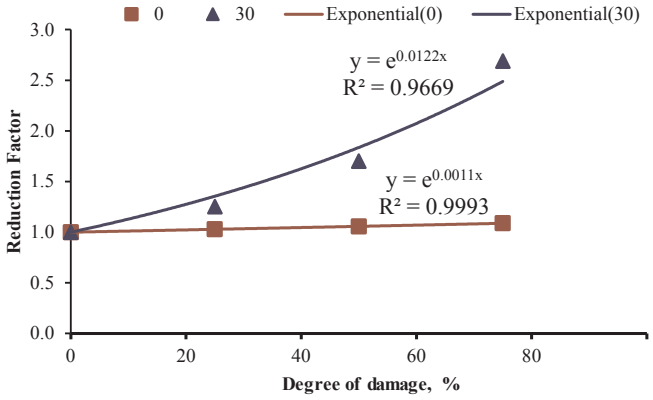

Fig. 14. RF_{ID} against degree of damage.

It can be seen in Fig. 3 that the pre-damaged geogrid under zero degree tension with the ultimate strength value of 28 kN/m had the highest tensile strength and stiffness. The second higher tensile strength and stiffness is the pre-damaged specimen under 90° tension with the ultimate strength value of 22.4 kN/m. The tensile strength and stiffness at 0°and 90°are much larger than those in other directions because the ribs at these orientations can provided stronger resistance.

Figs. 4 and 5 show the stress-strain curves of the pre-damaged geogrids at 50% and 75% degree of damage, respectively. As compared with the numerical results of the pre-damaged geogrids at 25% degree of damage, it can be found out that the pre-damaged geogrid has a similarly stress-strain response at a specific degree of damage. It also can be found out that the tensile stiffness (i.e. the initial slope) is constant for each pre-damaged geogrid at a certain loading direction except the geogrid at 45° loading.

Effect of degree of damage

Fig. 6 shows the stress-strain curves of different degree of damage under uniaxial tension at a specific loading direction (i.e., 0°, 30°, 45°, 60°, and 90°). Also the results of the intact geogrid (i.e., the degree of damage equals to zero) are listed in the same figure for the comparison purpose. All the curves are plotted using the average strain.

Fig. 6(a) shows the stress-strain curves of the pre-damaged geogrids subjected to 0-degree tension loading (i.e., same as the XMD). The tensile strength/stiffness decreased with the increase of the degree of damage. The value of ultimate tensile strength decreased from 28.80 kN/m to 28.00 kN/m, 27.19 kN/m, and 26.40 kN/m, respectively. It can be calculated that the losses of the ultimate tensile strength are 3%, 6%, and 8% at the degrees of damage of 25%, 50%, and 75% (i.e., the strength loss of the assigned geogrid ribs due to installation damage), respectively. The applied tensile force was mostly carried by the ribs parallel to the loading direction when subjected to 0-degree tension. The loss of the ultimate tensile strength was due to the strength loss of ribs (i.e., ribs in the middle of the whole test sheet along the cross-machine direction) due to installation damage.

Fig. 6(b) shows the stress-strain curves of the pre-damaged geogrids under 30-degree tension to the loading direction. With the increase of the degree of damage, the tensile strength and stiffness decreased significantly. At the degree of damage of 25%, 50%, and 75%, the ultimate tensile strengths were 2.73 kN/m, 1.98 kN/m, and 1.2 kN/m, respectively. As compared with the ultimate strength of 3.46 kN/m of the intact geogrid sheet, the losses of the ultimate tensile strength were 21%, 43%, and 65%, respectively. The larger loss of the tensile strength was due to the diagonal ribs (i.e., the damaged ribs) which were supposed to carry more load at higher strains. The higher strains along the diagonal ribs would lead to the quick failure of the whole geogrid specimen.

Fig. 6(c) shows the stress-strain curves of the pre-damaged geogrids subjected to 45-degree tension. At the initial stage of tension, the stress-strain curves are nearly the same with the increase of degree of damage. More obvious differences can be observed after the values of strains exceed 23%. The necking with excessive extension in the loading direction developed first before the damaged ribs worked.

Fig. 6(d) and 6(e) present the stress-strain curves of the pre-damaged geogrids subjected to 60-degree and 90-degree tension. Minor differences could be found in the stress-strain curves for the pre-damaged geogrids at different degree of damage. The slight differences show that the ribs carried the tensile loads when the geogrid subjected to 60-degree and 90-degree tension had little strength loss. The installation damage on the geogrid ribs in the middle of the whole test sheet along the cross-machine direction had little effect on the ultimate tensile strength.

Tensile strength/stiffness distributions

As shown in Figs. 3–5, the tensile stiffness (i.e. the initial slope) is constant from 0 to 6.4% for each geogrid at a certain loading direction except the geogrid at 45°loading. To investigate the effects of the degree of damage on the tensile strength/stiffness distributions, the numerical results are summarized in Figs. 7–12. Figs. 7–9 present the tensile strength distributions of the pre-damaged geogrid around 360° at a specific degree of damage (i.e., the dashed lines). Figs. 10–12 present the tensile stiffness distributions of the pre-damaged geogrid around 360° at a specific degree of damage (i.e., the dashed lines). The

distributions of the intact geogrid (i.e., the solid lines) are plotted in the same figure for the comparison purpose. An average strain of 5% which is typically used in practice was selected to determine the tensile strength/stiffness for all loading direction. Each point in the plot area represents the value of tensile strength/stiffness at certain loading direction. For example, the point at the positive horizontal axis in Fig. 7 represents the tensile strength value at 0° loading direction and determined at 5% average strain. The numbers (i.e. 0, 25, 50, and 75) in the figures represent the degree of damage.

Figs. 7 and 12 show that the tensile strengths/stiffness of the pre-damaged specimen is not only dependent on the loading direction relative to the orientation of ribs, but also dependent on the degree of damage. It can be observed that the tensile strength/stiffness at the 30° loading direction is more sensitive to the damage than the one at 0° loading direction. This result demonstrated that the resistance against 30° tension is mainly provided by the geogrid ribs in the middle of the whole test sheet along the XMD. Once the main ribs were damaged, the tensile strength/stiffness decreased sharply. This situation is more danger in the engineering practice. For the pre-damaged geogrid under 0° tension (cross-machine direction), all the geogrid ribs along XMD can provide resistance to the tension. Even the strength loss of the geogrid ribs in the middle of the whole sheet along the XMD reached 75%, the loss of the overall tensile strength was less than 10%. For the pre-damaged geogrid under 90° tension (machine direction), all the geogrid ribs along MD can provide resistance to the tension. The strength loss of the geogrid ribs in the middle of the whole sheet along the XMD had little effects on the overall tensile strength/stiffness. For the pre-damaged geogrid under 45° and 60° tension, the damage ribs along the middle of the whole sheet in the XMD hardly affected the overall tensile strength/stiffness.

Reduction factors due to installation damage

The results of the percentage of tensile strength retained (PT_R) and reduction factor (RF_{ID}) against installation damage are summarized in Tables 3 and 4, respectively. To investigate the effects of degree of damage on the tensile strength, the PT_R and RF_{ID} against the degree of damage at the loading direction of 0° and 30° are plotted in Figs. 13 and 14, respectively.

As listed in Table 3, the values of percentage of tensile strength retained (PT_R) at 0° tension due to installation damage ranged from 100% to 97%, 95%, and 92% with the degree of damage increased from 0% to 25%, 50%, and 75%, respectively. The relationship between PT_R and degree of damage at 0° tension can be observed in Fig. 13. Fig. 13 shows a linear trend with a R-squared value of 0.999. With the increase of degree of damage from 0% to 25%, 50%, and 75%, the reduction factor (RF_{ID}) against installation damage increased from 1.00 to 1.03, 1.06, and 1.09, as listed in Table 3, respectively. An exponential trend with a R-squared value of 0.999 is illustrated in Fig. 14.

For the pre-damaged geogrid under 30° tension, the values of PT_R listed in Table 2 ranged from 100% to 80%, 59%, and 37% as the degree of damage increased from 0% to 25%, 50%, and 75%, respectively. A linear relationship with a R-squared value of 0.999 between PT_R and degree of damage at 30° tension can be observed in Fig. 13. With the increase of degree of damage from 0% to 25%, 50%, and 75%, the RF_{ID} against installation damage increased from 1.00 to 1.25, 1.70, and 2.69, respectively. An exponential trend with a R-squared value of 0.966 is illustrated in Fig. 14.

Independent of the change of the degree of damage, the values of PT_R and RF_{ID} of the pre-damaged geogrid under 45°, 60°, and 90° tensions are 100% and 1.00, respectively. .

The largest range of RF_{ID} of geogrid suggested by Koerner [15] is 1.2-1.5. Except for the pre-damaged geogrid under 30° tension, all the RF_{ID} are within this range. For the pre-damaged geogrid specimen under 30° tension, the RF_{ID} already reached 1.70 at the damage of 50%. Thus, a higher RF_{ID} due to installation damage is suggested when a geogrid is subjected 30° tension relative to the orientation of ribs.

Conclusions

The tensile behavior of a pre-damaged geogrid with rectangular apertures under uniaxial tension at different loading directions was investigated using the numerical software FLAC 2D. Certain degree of damage was assigned to the geogrid ribs to model a geogrid sample at different installation damage conditions. Only the geogrid ribs in the middle of the whole test sheet along the cross-machine direction (XMD direction) was pre-damaged. Several conclusions can be drawn based on the above numerical analysis:

(1) The numerical study demonstrated that the pre-damaged geogrid with rectangular apertures had similar stress-strain responses at a specific degree of damage when it was subjected to tension at the loading directions. The pre-damaged geogrids under 30° tension had the highest sensitivity to the damage. With the increase of the degree of damage, the tensile strengths decreased relative quickly.
(2) An increase of the degree of installation damage of ribs decreased the tensile strength/stiffness of the geogrid with rectangular apertures.
(3) The pre-damaged geogrid subjected to 0° and 30° tension had a linear relationship between the percentages of tensile strength retained and the degrees of damage. There was an exponential relationship between the reduction factors and the degrees of damage.
(4) A higher RF_{ID} value due to installation damage is suggested when a geogrid was subjected 30° tension relative to the orientation of ribs.

Acknowledgements

This work was supported by the project of National Natural Science Fund for the Youth, China (No. 51208473, 51608316), and the project of Natural Science Fund of Shanxi for the Youth, China (No. 2012021019-1). These sponsorships are greatly appreciated.

References

[1] Bush DI. Evaluation of the effects of construction activities on the physical properties of polymeric soil reinforcing elements. In: Proceedings of the International Geotechnical Symposium on Theory and Practice of Earth Reinforcement, Fukuoka, Japan: 1988;63–8.
[2] Dong YL, Han J, Bai XH. A numerical study on stress-strain responses of biaxial geogrids under tension at different directions. Adv Anal Model Des Geotech Spec Publ 2010;199:2551–60.
[3] Dong YL, Han J, Bai XH. Numerical analysis of tensile behavior of geogrids with rectangular and triangular apertures. Geotextiles Geomembranes 2011;29:83–91.
[4] Han J, Gabr MA. Numerical analysis of geosynthetic-reinforced and pile supported earth platforms over soft soil. J Geotech Geoenviron Eng 2002;128(1):44–53.
[5] Hsieh CW, Wu JH. Installation survivability of flexible geogrids in various pavement subgrade materials. Transp Res Rec 2001;1772:190–6.
[6] Huang CC. Laboratory simulations of installation damage of a geogrid. Geosynthetics Int 2006;13(3):120–32.
[7] Huang CC, Chiou SL. Investigation of installation damage of some geogrids using laboratory tests. Geosynthetics Int 2006;13(1):23–35.
[8] Huang CC, Wang ZH. Installation damage of geogrids: influence of load intensity. Geosynthetics Int 2007;14(2):65–75.
[9] Huang J, Han J, Oztoprak S. Coupled mechanical and hydraulic modeling of geosynthetic-reinforced column-supported embankments. J Geotech Geoenviron Eng 2009;135(8):1011–21.
[10] Hufenus R, Rüegger R, Flum D, Sterba IJ. Strength reduction factors due to installation damage of reinforcing geosynthetics. Geotextiles Geomembranes 2005;23(5):401–24.
[11] Paula AM, Pinho-Lopes M, Lopes ML. Damage during installation laboratory test: influence of the type of granular material. Proceedings of the 3rd European Geosynthetics Conference: 2004;603–606.
[12] Rainey T, Barksdale B. Construction induced reduction in tensile strength of polymer geogrids. Proceedings of the Geosynthetics '93 Conference, Vancouver, Canada: 1993;729–742.
[13] Troost GH, Ploeg NA. Influence of weaving structure and coating on the degree of mechanical damage of reinforcing mats and woven geogrids, caused by different fills, during installation. Proceedings of the 4th International Conference Geotextiles, Geomembranes and Related Products, The Hague, The Netherlands: 1990;609–14.
[14] Watts GRA, Brady KC. Geosynthetics: installation damage and the measurement of tensile strength. Proceedings of the 5th International Conference on Geotextiles and Related Products, Singapore: 1994;1159–164.
[15] Koerner RM. Designing with Geosynthetics. 4th ed. New York: Prentice Hall; 1998.